ELSEVIER

Materials Science and Engineering A 445–446 (2007) 486–492

MATERIALS SCIENCE & ENGINEERING A

www.elsevier.com/locate/msea

Electrical discharge machining of TiNiCr and TiNiZr ternary shape memory alloys

S.L. Chen [a,*], S.F. Hsieh [b], H.C. Lin [c], M.H. Lin [a], J.S. Huang [b]

[a] *Department of Mechanical Engineering, National Kaohsiung University of Applied Sciences, Kaohsiung, Taiwan 807, Republic of China*
[b] *Department of Mold and Die Engineering, National Kaohsiung University of Applied Sciences, Kaohsiung, Taiwan 807, Republic of China*
[c] *Department of Materials Science and Engineering, National Taiwan University, Taipei, Taiwan 106, Republic of China*

Received 10 July 2006; accepted 22 September 2006

Abstract

This study investigates the influence of the machining characteristics on TiNiX ternary shape memory alloys (SMAs) using electro-discharge machining (EDM). Experimental results show that the material removal rates (MRRs) of $Ti_{50}Ni_{49.5}Cr_{0.5}$ and $Ti_{35.5}Ni_{49.5}Zr_{15}$ alloys in the EDM process exhibit a reverse relationship to the product of the alloy's melting temperature and thermal conductivity. The surface roughness (R_a) of the EDMed TiNiX alloys is found to obey the empirical equation of $R_a = \beta(I_P \times \tau_P)^{\alpha}$. Having a less $T_\Theta \times K_T$ value, $Ti_{50}Ni_{49.5}Cr_{0.5}$ alloy has a larger R_a value than that of $Ti_{35.5}Ni_{49.5}Zr_{15}$ alloy after electro-discharge machining. Besides, a lower discharge current I_P and a shorter pulse duration τ_P should be selected to have a precise EDM machining of TiNiX SMAs. The hardening effect near the outer surface for EDMed TiNiX alloys originates from the recast layer. The thickness of the recast layer varies with the pulse duration and exhibits a minimum value at the maximal MRR. The EDMed TiNiX alloys still exhibit a nearly perfect shape recovery at a normal bending strain, but slight degradation of shape recovery occurs at a higher bending strain due to the constrained effect on the TiNiX matrix by the recast layer.

Keywords: EDM; Roughness; Ti–Ni shape memory alloys

1. Introduction

Although TiNi alloys are the most widely used shape memory alloys (SMAs), to extend their specific needs in various application fields, some TiNiX ternary alloys still need to be developed and studied. The addition of a third element to replace Ni and/or Ti in TiNi alloys has a substantial effect on their phase transformation behaviors. The Ms temperature decreases monotonously following the substitution of Ni with Cr, V, Fe, Mn and Co elements [1–4], but increases remarkably following the substitution of Ni with Au, Pd and Pt in amounts not less than 15–20 at.% [5–7]. On the other hand, the addition of Cr in a TiNi alloy can widen the transformation temperature range [8]. Wide thermal hysteresis is desirable for coupling and sealing applications. However, the applications of these alloys are limited to use at temperatures lower than 100 °C. For this reason, high-temperature SMAs need to be investigated. Among them, the most significant candidates are TiNiZr and TiNiHf alloys, where Zr and Hf are used to replace Ti in these alloys [9–13].

The roadblocks to TiNi SMAs development are caused by difficulties in the manufacturing process. It is well known that TiNi alloys can be tensile-deformed in a ductile manner to about 50% strain prior to fracture, but the severe strain hardening and the unique pseudoelastic behavior have caused the machining characteristics of TiNi SMAs to be quite complicated [14]. To overcome this difficulty, some special techniques, such as the electro-discharge machining (EDM) and laser machining, may exhibit an excellent ability in machining the TiNi SMAs [15]. EDM is an electro-thermal process in which the material is removed by electro-discharges occurring between the work-piece and tool electrode immersed in a liquid dielectric medium. These electro-discharges melt and vaporize minute amounts of the work-piece, which are then swept away by the dielectric. Therefore, EDM is a versatile technique in machining the stubborn materials, which are difficult to machine by conventional techniques. To extend the applications of TiNiX ternary SMAs, some machining technologies for production of complicated shapes with high accuracy should be urgently developed. Hence,

* Corresponding author. Tel.: +886 7 381 4526x5342; fax: +886 7 383 1373.
E-mail address: slchen@cc.kuas.edu.tw (S.L. Chen).

0921-5093/$ – see front matter © 2006 Elsevier B.V. All rights reserved.
doi:10.1016/j.msea.2006.09.109

Table 1
The machining parameters of EDM in this study

Discharge current (A)	3, 6, 10, 19
Pulse duration (μs)	3, 6, 12, 25, 50, 100
Pause duration (μs)	3, 6, 12, 25, 50, 100
Gap voltage (V)	50
Electrode	Cu (+); work-piece (−)
Dielectric	Kerosene

the aim of the present work is to investigate the machining characteristics of TiNiCr and TiNiZr alloys involving EDM. The microstructure, composition, hardness and roughness of EDMed surfaces are also discussed.

2. Experimental procedure

The conventional tungsten arc-melting technique was employed to prepare the $Ti_{50}Ni_{49.5}Cr_{0.5}$ and $Ti_{35.5}Ni_{49.5}Zr_{15}$ alloys. Titanium (purity, 99.7 wt.%), nickel (purity, 99.9 wt.%), chromium (purity, 99.9 wt.%) and zirconium (purity, 99.8 wt.%), totaling about 180 g, were melted and remelted at least six times in an argon atmosphere. Pure titanium buttons were also melted and used as getters. The mass loss during melting was negligibly small. The as-melted buttons were homogenized at 950 °C in a 7×10^{-6} Torr vacuum furnace for 72 h. The homogenized buttons were cut into several plates with a low speed diamond saw. Specimens for the electro-discharge machining (size: 55 mm × 20 mm × 5 mm) were carefully cut and ground from these plates. These specimens were annealed at 900 °C for 2 h in a vacuum furnace and then quenched in water.

The EDM specimens were performed on a die-sinking EDM machine model type 30-TP, made by Topedm Co. in Taiwan. The operation parameters used in this study are presented in Table 1. The microstructures of electro-discharge machined (EDMed) surfaces were examined using X-ray diffraction (XRD), scanning electron microscopy (SEM) and secondary electron image (SEI). The X-ray analyses of EDMed surfaces were performed at room temperature by a Siemens D5000 XRD using Cu Kα radiation. The power was 30 kV × 20 mA and the 2θ scanning rate was 3° min^{-1}. The morphologies of EDMed surface were observed using a JEOL 6330 TF SEM with SEI facility. A precision profilometer was used to evaluate quantitatively the roughness of the EDMed surface, presented by R_a. The surface hardness was measured in a microvickers hardness tester with a load of 25 g for 15 s. For each specimen, the average hardness value was taken from at least five test readings. The shape memory effect (SME) of these EDMed TiNiX alloys was examined by a bending test [16].

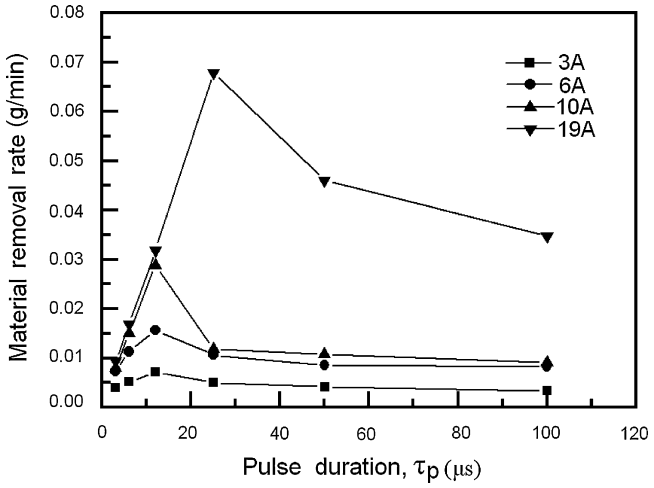

Fig. 1. The material removal rate vs. the pulse duration τ_P at various discharge currents I_P for the $Ti_{50}Ni_{49.5}Cr_{0.5}$ alloy.

3. Results and discussion

3.1. The material removal rate and surface roughness of TiNiX SMAs after EDM process

Table 2 presents the transformation temperatures, hardness and crystal structures at room temperature for $Ti_{50}Ni_{49.5}Cr_{0.5}$ and $Ti_{35.5}Ni_{49.5}Zr_{15}$ ternary SMAs. Some important metallurgical properties of these alloys in Table 2 are helpful to investigate machining characteristics of TiNiX alloys in the EDM process. From this table, one can find that $Ti_{50}Ni_{49.5}Cr_{0.5}$ and $Ti_{35.5}Ni_{49.5}Zr_{15}$ SMAs exhibit the mixture of Ti_2(Ni, Cr), R-phase and B2, and (Ti, Zr)$_2$Ni, λ_1-phase and B19′-phase, respectively. In addition to the material intrinsic properties, many machining parameters such as the electrode polarity, discharge current I_P, pulse duration τ_P and electrode material, can significantly influence the EDM characteristics.

In the present study, we hope to determine the influence of some of the most important parameters implicated in the EDM process on $Ti_{50}Ni_{49.5}Cr_{0.5}$ and $Ti_{35.5}Ni_{49.5}Zr_{15}$ ternary alloys including discharge current I_P and pulse duration τ_P. Fig. 1 shows the material removal rate (MRR) versus the pulse duration at various discharge currents for the $Ti_{50}Ni_{49.5}Cr_{0.5}$ alloy. It is found that the MRR increases with the discharge current. It has been reported that a high discharge current can have a high current density [17]. This feature will obviously increase the material's melting and evaporation and the impulsive force of expanded dielectric medium. Therefore, a higher MRR occurs at a higher discharge current during the EDM process. Besides, one can also find in Fig. 1 that the MRRs initially increase with

Table 2
The crystal structures and some basic properties of $Ti_{50}Ni_{49.5}Cr_{0.5}$ and $Ti_{35.5}Ni_{49.5}Zr_{15}$ ternary alloys

Alloy	M* (°C)	A* (°C)	Hardness (Hv)	Crystal structure
$Ti_{50}Ni_{49.5}Cr_{0.5}$	22 (B2 → R), 10(R→B19′)	54 (R → B2), 42(B19′ → R)	290	R-phase + Ti_2(Ni, Cr) + B2
$Ti_{35.5}Ni_{49.5}Zr_{15}$	176	217	320	B19′ + λ_1-phase + (Ti, Zr)$_2$Ni

M*, A*: DSC peak temperatures of forward and reverse martensitic transformations, respectively.

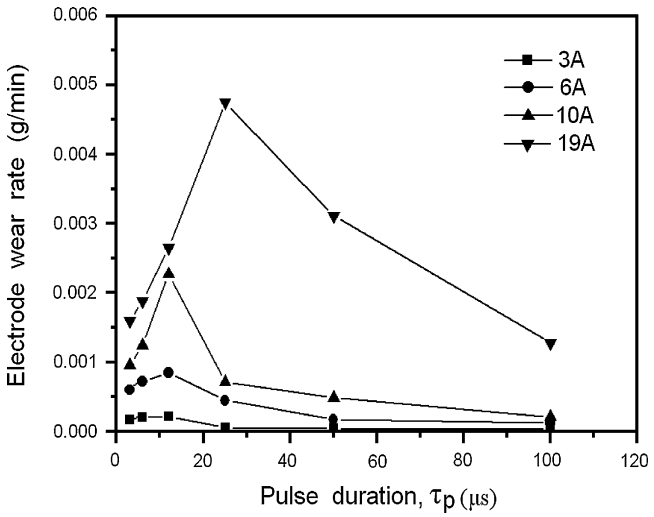

Fig. 2. The electrode wear rate vs. the pulse duration τ_P at various discharge currents I_P for the $Ti_{50}Ni_{49.5}Cr_{0.5}$ alloy.

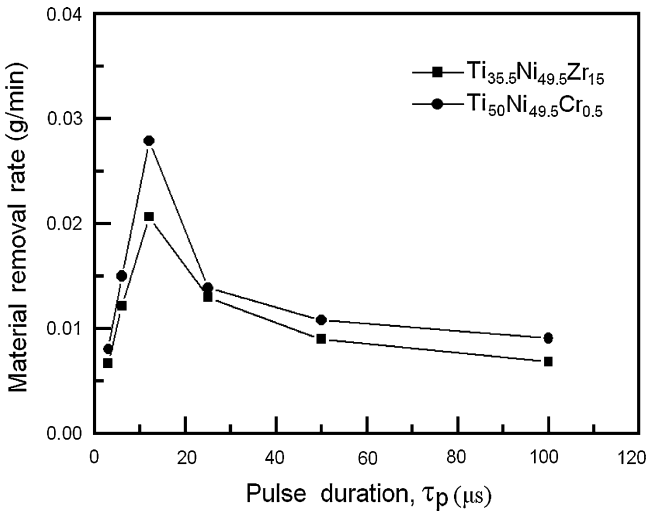

Fig. 3. The material removal rate vs. the pulse duration τ_P at $I_P = 10$ A for the $Ti_{50}Ni_{49.5}Cr_{0.5}$ and $Ti_{35.5}Ni_{49.5}Zr_{15}$ alloys.

the pulse duration, reach maximum values, and then decrease to constant values for various discharge currents. It is expected that the MRR should increase with growing pulse duration, because its high accumulated electro-discharge energy will rapidly melt and evaporate the material. Moreover, an over-long pulse duration will reduce the energy density of the discharge spots by expanding the plasma channel [18]. The energy provided by the plasma channel melts the material, but it is insufficient to generate a high exploding pressure of the dielectric which can flush the molten materials away from the EDMed surface. As a consequence, the molten material cannot be swept away effectively by the circulative dielectric system, and hence the MRR decreases.

As well as the work-piece, the Cu electrode will also slightly melt and evaporate during EDM. To possess the high accuracy and efficiency of EDM, it is important to understand the consumption of electrode material. Fig. 2 depicts the electrode wear rate (EWR) versus the pulse duration at various discharge currents for the $Ti_{50}Ni_{49.5}Cr_{0.5}$ alloy. It indicates that the EWR initially increases, reaches a maximum value and then decreases with growing pulse duration. This variation of the EWR with pulse duration reveals a similar tendency to that of the MRR with pulse duration shown in Fig. 1. The electro-discharge energy mode also has a significant effect on the EWR. In addition, it is worthy to mention that the variations of the MRR and EWR with discharge current and pulse duration for the $Ti_{35.5}Ni_{49.5}Zr_{15}$ alloy are similar to those shown in Figs. 1 and 2 for the $Ti_{50}Ni_{49.5}Cr_{0.5}$ alloy. These features can conclude that the $Ti_{50}Ni_{49.5}Cr_{0.5}$ and $Ti_{35.5}Ni_{49.5}Zr_{15}$ alloys exhibit similar EDM characteristics although they have different mechanical properties and crystal structures at room temperature.

Fig. 3 depicts the MRR versus the pulse duration at $I_P = 10$ A for $Ti_{50}Ni_{49.5}Cr_{0.5}$ and $Ti_{35.5}Ni_{49.5}Zr_{15}$ alloys. From Fig. 3, the MRR of $Ti_{50}Ni_{49.5}Cr_{0.5}$ alloy is larger than that of $Ti_{35.5}Ni_{49.5}Zr_{15}$ alloy at various pulse durations during the EDM process. This characteristic is associated with their melting temperature (T_Θ) and thermal conductivity (K_T). Materials with higher melting temperature, leading to less melting and evaporation, and higher thermal conductivity, causing more heat transfer of discharge energy to the nearby matrix, will exhibit a lower MRR in the EDM process. The same characteristic shown in Fig. 3 also occurs when electro-discharge machining $Ti_{50}Ni_{50}$ and $Ti_{49}Ni_{51}$ binary alloys [19]. Hence, the product of the melting temperature and thermal conductivity of materials can be used to estimate the EDM characteristic in TiNiX alloys. We propose that the MRR may have a reverse relationship to the product of the materials' melting temperature and thermal conductivity. Table 3 presents the product of the melting temperature and thermal conductivity of $Ti_{50}Ni_{50}$, $Ti_{49}Ni_{51}$ binary alloys, and $Ti_{50}Ni_{49.5}Cr_{0.5}$, $Ti_{35.5}Ni_{49.5}Zr_{15}$ ternary alloys. Upon carefully examining Fig. 3 and Table 3, the MRRs of $Ti_{50}Ni_{49.5}Cr_{0.5}$ and $Ti_{35.5}Ni_{49.5}Zr_{15}$ alloys coincide with the above mentioned relationship. Based on Table 3 and Ref. [19], the products $T_\Theta \times K_T$ for TiNi binary alloys and TiNiX ternary alloys show the sequence of $Ti_{50}Ni_{50} < Ti_{51}Ni_{49} < Ti_{50}Ni_{49.5}Cr_{0.5} < Ti_{35.5}Ni_{49.5}Zr_{15}$, and hence the MRRs will have the sequence of $Ti_{50}Ni_{50} > Ti_{51}Ni_{49} > Ti_{50}Ni_{49.5}Cr_{0.5} > Ti_{35.5}Ni_{49.5}Zr_{15}$.

As mentioned above, the electro-discharge energy mode in the EDM process, involving the discharge current I_P and pulse duration τ_P, can also affect the work material's surface roughness. Fig. 4 depicts the roughness of EDMed surface versus the pulse duration at various discharge currents for $Ti_{50}Ni_{49.5}Cr_{0.5}$ alloy. The variation tendency of EDMed surface roughness for $Ti_{35.5}Ni_{49.5}Zr_{15}$ alloy is similar to those shown in Fig. 4 and is omitted here. These features demonstrate that the higher dis-

Table 3
The product of the melting temperature and thermal conductivity of TiNi binary alloys and TiNiX ternary alloys

Alloy	$T_\Theta \times K_T$ (W cm^{-1} °C^{-1})
$Ti_{50}Ni_{50}$	111.8
$Ti_{51}Ni_{49}$	234.0
$Ti_{50}Ni_{49.5}Cr_{0.5}$	310.1
$Ti_{35.5}Ni_{49.5}Zr_{15}$	470.4

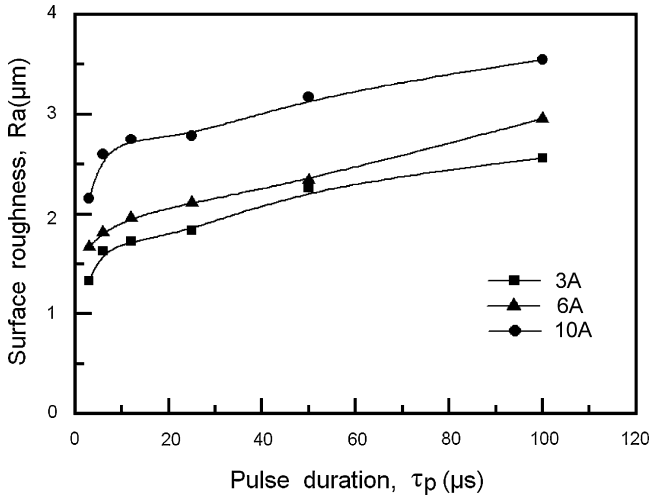

Fig. 4. The surface roughness vs. the pulse duration τ_P at various discharge currents I_P for the $Ti_{50}Ni_{49.5}Cr_{0.5}$ alloy.

charge current and pulse duration will have higher roughness of EDMed surface. As the discharge current increases, discharges strike the surface of the work-piece more intensely, and the resulting worsened erosion effect leads to a deterioration of the surface roughness. Furthermore, an extended pulse duration allows greater discharge energy to melt and penetrate deeper into the material, which produces deeper and larger craters, causing an increased surface roughness on the work-piece.

Fig. 5 shows the surface roughness R_a versus the product of the discharge current I_P and pulse duration τ_P for $Ti_{50}Ni_{49.5}Cr_{0.5}$ and $Ti_{35.5}Ni_{49.5}Zr_{15}$ ternary alloys. The roughness of an EDMed surface increases with growing pulse energy. This feature is found to obey an empirical equation of $R_a = \beta(I_P \times \tau_P)^{\alpha}$, where the constants β and α depend on the tool-work material combination, including the electrode materials, work material's structures, mechanical properties, thermal properties and the electro-discharge energy mode [20,21]. From the curves shown in Fig. 5, the roughness of the EDMed surface is found to follow the equation $R_a = 11.83(I_P \times \tau_P)^{0.18}$ for $Ti_{50}Ni_{49.5}Cr_{0.5}$ alloy, but

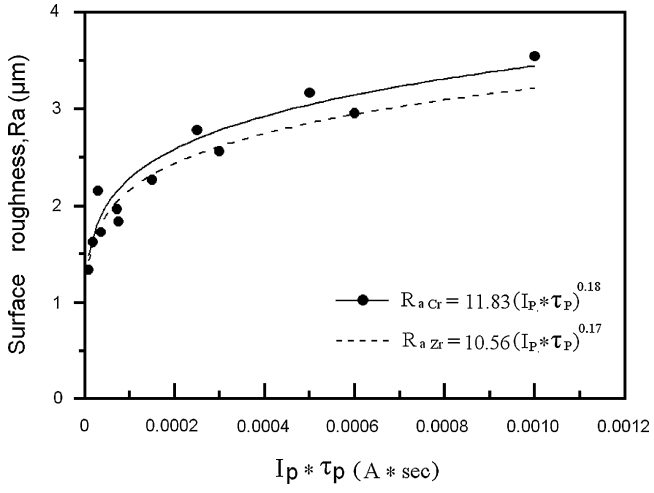

Fig. 5. The surface roughness vs. the product of I_P and τ_P for the EDMed $Ti_{50}Ni_{49.5}Cr_{0.5}$ and $Ti_{35.5}Ni_{49.5}Zr_{15}$ alloys.

$R_a = 10.56(I_P \times \tau_P)^{0.17}$ for $Ti_{35.5}Ni_{49.5}Zr_{15}$ alloy. The values of the constants β and α were determined by fitting the curve by the least-squares method. The R_a value of $Ti_{35.5}Ni_{49.5}Zr_{15}$ alloy after electro-discharge machining is less than that of $Ti_{50}Ni_{49.5}Cr_{0.5}$ alloy, as shown in Fig. 5. We propose that the R_a value is also related to the materials' melting temperature and thermal conductivity in TiNiX SMAs. The greater the $T_\Theta \times K_T$ value is, the less the MRR and R_a value will be. In other words, the roughness of the EDMed surface is larger for the alloy having a lower $T_\Theta \times K_T$ value.

3.2. Surface topography and composition analysis of TiNiX SMAs after EDM process

Surface topography of $Ti_{50}Ni_{49.5}Cr_{0.5}$ and $Ti_{35.5}Ni_{49.5}Zr_{15}$ ternary SMAs after EDM process is presented in Fig. 6. It is characterized by discharge craters, melting drops (globules of debris) and recast materials. Fig. 7 shows the XRD patterns of the EDMed surface layer for the $Ti_{50}Ni_{49.5}Cr_{0.5}$ and $Ti_{35.5}Ni_{49.5}Zr_{15}$ alloys. It indicates that the EDMed surface layer consists of Cr_2O_3, TiO_2, $TiNiO_3$, C, TiC, Cu_2O, ZrO_2 and Ni-

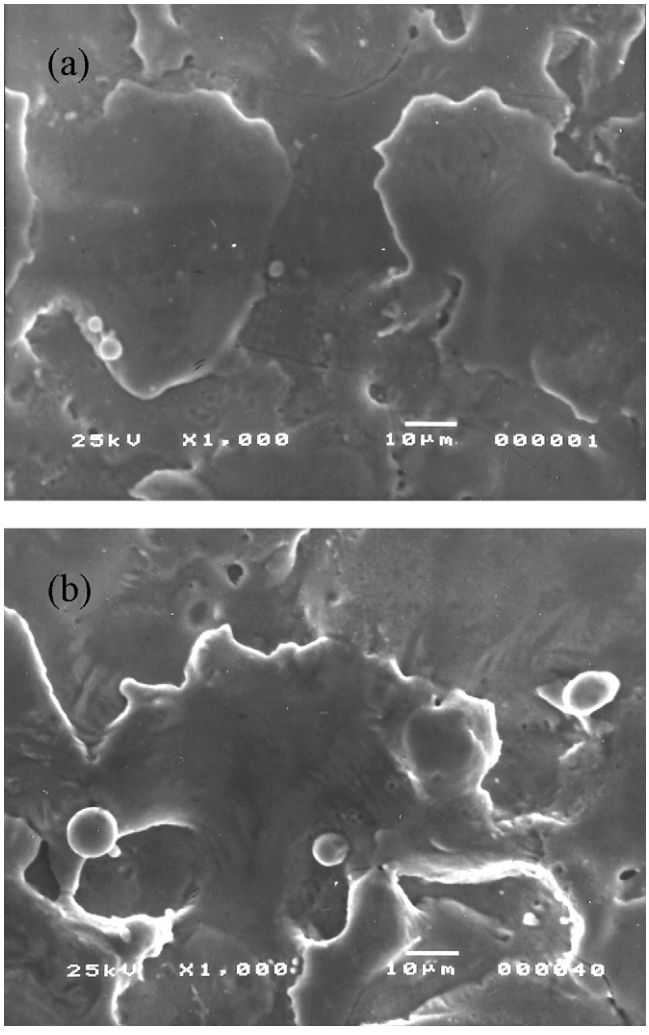

Fig. 6. The SEM micrographs of the EDMed surface for (a) $Ti_{50}Ni_{49.5}Cr_{0.5}$ alloy and (b) $Ti_{35.5}Ni_{49.5}Zr_{15}$ alloy.

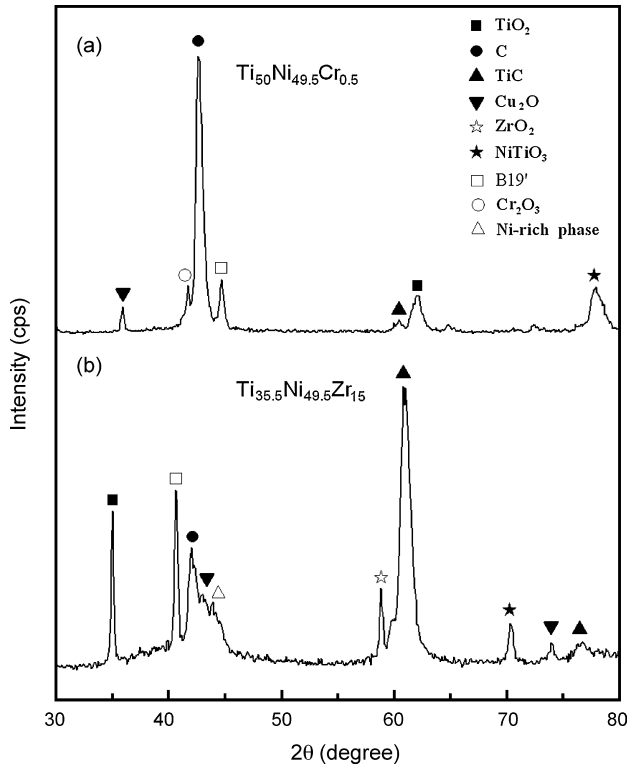

Fig. 7. The XRD patterns of the EDMed surface layer for (a) $Ti_{50}Ni_{49.5}Cr_{0.5}$ alloy and (b) $Ti_{35.5}Ni_{49.5}Zr_{15}$ alloy.

rich phase. From Fig. 7(a), the formation of TiO_2, $TiNiO_3$ and Cr_2O_3 oxides is ascribed to the high activity of Ti, Ni and Cr atoms. Cu_2O and C are due to the deposition of the consumed Cu electrode and kerosene dielectric medium. Thus, the evaporated Ti and C atoms have a great chemical affinity to form TiC carbides deposited on the EDMed surface. In the meantime, because Ti atoms are exhausted in forming the TiO_2 and TiC particles, the residual Ni atoms diffuse into the TiNi matrix to form the Ni-rich regions. The similar phenomenon can be also found in $Ti_{35.5}Ni_{49.5}Zr_{15}$ alloy, as shown in Fig. 7(b).

As mentioned above, lots of recast materials deposit on the EDMed surface of TiNiX alloys. Fig. 8a–d reveal the cross-sectional SEI micrographs near the EDMed surface layer for the $Ti_{50}Ni_{49.5}Cr_{0.5}$ alloy under the conditions of $I_P = 10$ A and $\tau_P = 3, 6, 12, 50$ μs, respectively. The cross-sectional SEI micrographs near the EDMed surface layer for the $Ti_{35.5}Ni_{49.5}Zr_{15}$ alloy are similar to those shown in Fig. 8a–d and are omitted here. Carefully examining Fig. 8a–d, the thickness of the recast layer varies with the pulse duration. There appears a thicker recast layer at shorter pulse duration ($\tau_P = 3$, 6 μs), drops to a minimum value as well as a maximum MRR at $\tau_P = 12$ μs, and then the thickness increases again in the extended pulse duration ($\tau_P = 50$ μs). It can be explained as below. During EDM process, the electrode-discharge plasma channel is composed of electron and ion flows. In the early stage, the electron flow is dominant in the plasma channel and hence the cathode (work-piece) has lower electro-discharge energy. At the same time, the ratio of positive ions flow in the plasma channel increases with growing pulse duration [17] and the electro-discharge energy of the work-piece increases, and hence the thickness of the recast layer grows in the beginning pulse duration (≤6 μs). Thereafter, for the optimal pulse duration at the maximal MRR, the high electro-discharge energy will also make the dielectric medium have violent impact force to effectively repel the molten materials and the deposited particles from the EDMed surface, and hence

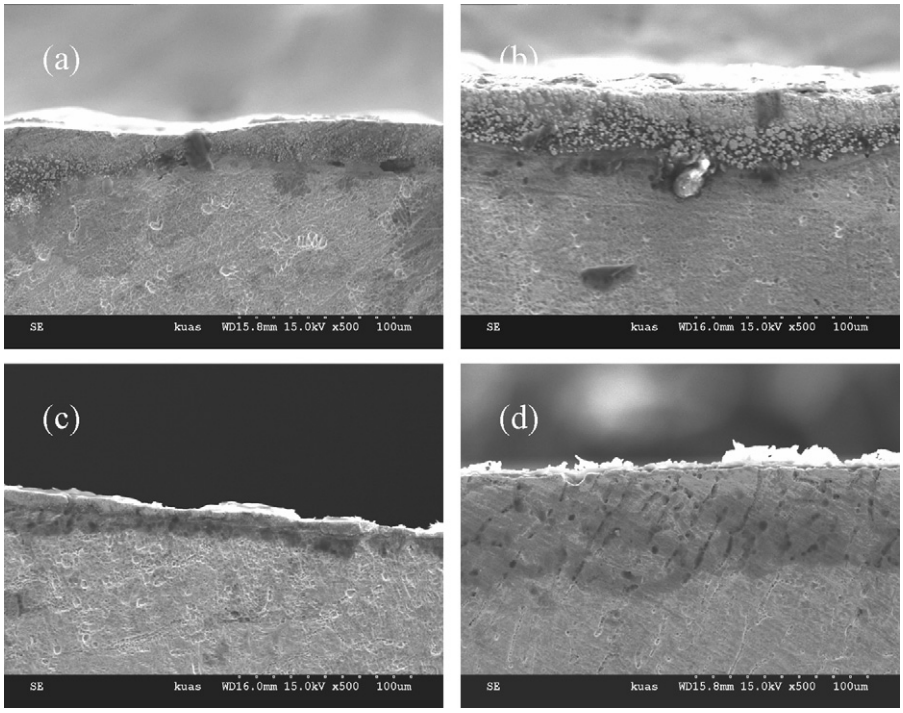

Fig. 8. The cross-sectional SEI micrographs near the EDMed surface layer for the $Ti_{50}Ni_{49.5}Cr_{0.5}$ SMA under the conditions of $I_P = 10$ A and τ_P (a) 3 μs, (b) 6 μs, (c) 12 μs, and (d) 50 μs.

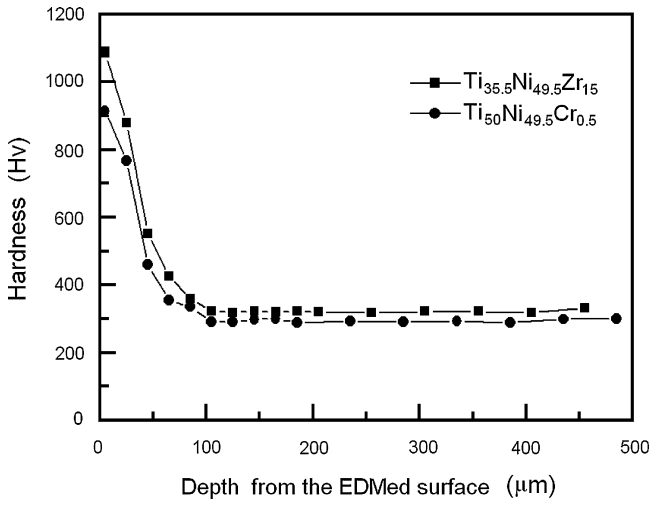

Fig. 9. The specimen's hardness at various distance from the EDMed surfaces of TiNiX ternary SMAs under the condition $I_P = 10$ A and $\tau_P = 100$ μs.

the recast layer is getting thinner, as shown in Fig. 8(c). As to, an over-long pulse duration will have relatively high accumulated electro-discharge energy. This makes more material be melted and re-solidified, as well as more kerosene dielectric medium be dissolved and deposited on the EDMed surface. If this molten material is not swept away from the surface by the dielectric, it will solidify during the cooling process and form a recast layer. Therefore, the thickness of the recast layer is increased again. Based on the above discussion, a lower discharge current I_P and a shorter pulse duration τ_P should be selected to have a precise EDM machining of TiNiX ternary SMAs, but this approach is more time consuming.

3.3. The shape recovery ability near EDMed surfaces of TiNiX ternary alloys

Fig. 9 shows the cross-sectional hardness versus distance form the EDMed surfaces of $Ti_{50}Ni_{49.5}Cr_{0.5}$ and $Ti_{35.5}Ni_{49.5}Zr_{15}$ alloys under the conditions of $I_P = 10$ A and $\tau_P = 100$ μs. It indicates that the specimen's hardness near the outer surface can reach 913 Hv for $Ti_{50}Ni_{49.5}Cr_{0.5}$ alloy, but 1087 Hv for $Ti_{35.5}Ni_{49.5}Zr_{15}$ alloy. This hardening effect is due to the formation of the oxides Cr_2O_3, ZrO_2, TiO_2, $TiNiO_3$, carbides TiC and the deposition particles in the recast layer. Besides, the hardness of the matrix in TiNiX alloys is not affected by the EDM process.

Table 4 depicts the measured shape recovery near the EDMed surface of the $Ti_{50}Ni_{49.5}Cr_{0.5}$ and $Ti_{35.5}Ni_{49.5}Zr_{15}$ alloys. The specimen's thickness for SME test is 0.6 mm, which is much thicker than the recast layer (<100 μm). It shows in Table 4 that the EDMed alloys exhibit almost perfect shape recovery at 3 and 5% bending strains, but a slightly reduced shape recovery at 8% bending strains, as compared with that of as-annealed TiNiX alloys. This feature indicates that the recast layer formed during the EDMed process has no obvious effect to depress the shape recovery of these alloys at normal bending strains. Thus, at higher bending strains, the shape recovery will be slightly reduced because the recast layer does not exhibit the shape memory effect. Furthermore, their constrained effect of the recast layer on the matrix will also depress the shape recovery of the matrix on TiNiX alloys. Therefore, in the application of thin plates, the recast layer on the EDMed surface of TiNiX SMAs should be mechanically ground and/or machined by electrochemical polishing before the SME treatment to improve their shape recovery characteristics.

Table 4
The measured shape recovery near the EDMed surface of $Ti_{50}Ni_{49.5}Cr_{0.5}$ and $Ti_{35.5}Ni_{49.5}Zr_{15}$ alloys

Alloy	Shape recovery (%)		
	$\varepsilon = 3\%$	$\varepsilon = 5\%$	$\varepsilon = 8\%$
$Ti_{50}Ni_{49.5}Cr_{0.5}$ (as-annealed)	100	100	90
$Ti_{50}Ni_{49.5}Cr_{0.5}$ (EDMed)	100	99	83
$Ti_{35.5}Ni_{49.5}Zr_{15}$ (as-annealed)	100	100	88
$Ti_{35.5}Ni_{49.5}Zr_{15}$ (EDMed)	100	98	82

4. Conclusion

The MRRs of $Ti_{50}Ni_{49.5}Cr_{0.5}$ and $Ti_{35.5}Ni_{49.5}Zr_{15}$ ternary SMAs in the EDM process significantly relate to the electro-discharge energy mode. It increases monotonically with growing discharge current, but appears a maximum value at an optimal pulse duration, saying $\tau_P = 12$ μs at $I_P = 10$ A in this study. Besides, their MRRs are found to have a reverse relationship to the product of the material's melting temperature and thermal conductivity. The roughness of EDMed surface increases with the discharge current and pulse duration, and follows the empirical equation $R_a = \beta(I_P \times \tau_P)^{\alpha}$. The $Ti_{50}Ni_{49.5}Cr_{0.5}$ alloy, having a less $T_\Theta \times K_T$ value, exhibits a rougher EDMed surface than that of $Ti_{35.5}Ni_{49.5}Zr_{15}$ alloy. The thickness of the recast layer for the EDMed TiNiX alloys varies with the pulse duration and exhibits a minimum value at the maximal MRR. The specimen's hardness near the outer surface can reach 913 and 1087 Hv for EDMed $Ti_{50}Ni_{49.5}Cr_{0.5}$ and $Ti_{35.5}Ni_{49.5}Zr_{15}$ alloys, respectively. This hardening effect is due to the formation of the oxides Cr_2O_3, TiO_2, $TiNiO_3$, ZrO_2, carbides TiC, and the deposition particles of the consumed Cu electrode and dissolved dielectric medium in the recast layer. The EDMed TiNiX alloys still exhibit a nearly perfect shape recovery at a normal bending strain, but a slightly reduced shape recovery at a higher bending strain due to their constrained effect on the TiNiX matrix by the recast layer.

Acknowledgement

The authors sincerely acknowledge the financial support of this research by the National Science Council (NSC), Republic of China, under the Grant NSC 94-2212-E-151-013.

References

[1] K.H. Eckelmeyer, Scripta Metall. 10 (1976) 667–672.
[2] R. Wasilewski, in: J. Perkin (Ed.), Shape Memory Effects in Alloys, Plenum, New York, 1975, p. 245.

[3] C.M. Hwang, M. Meichle, M.B. Salamon, C.M. Wayman, Philos. Mag. 47A (1983) 9–30.
[4] V.I. Kolomystev, Scripta Metall. 31 (1994) 1415–1420.
[5] S.K. Wu, C.M. Wayman, Metallography 20 (1987) 359–376.
[6] Y.C. Lo, S.K. Wu, C.M. Wayman, Scripta Metall. 24 (1990) 1571–1576.
[7] P.G. Lindqist, C.M. Wayman, in: T.W. Duering, K.N. Melton, D. Stockel, C.M. Wayman (Eds.), Engineering Aspects Of Shape Memory Alloys, Butterworth-Heinenmann, London, 1990, p. 58.
[8] J. Uchil, K.G. Kumara, K.K. Mahesh, J. Alloys Compd. 325 (2001) 210–214.
[9] J.H. Mulder, J.H. Mass, J. Beyer, ICOMAT (1992) 869–874.
[10] S.K. Wu, S.F. Hsieh, J. Alloys Compd. 297 (2000) 294–302.
[11] F. Dalle, E. Perrin, P. Vermaut, M. Masse, R. Portier, Acta Mater. 50 (2002) 3557–3565.
[12] S.F. Hsieh, S.K. Wu, Mater. Charact. 45 (2000) 143–152.
[13] S.F. Hsieh, W.K. Chang, J. Mater. Sci. 37 (2000) 2851–2856.
[14] H.C. Lin, K.M. Lin, Y.C. Chen, J. Mater. Process. Technol. 105 (2000) 327–332.
[15] W. Theisen, A. Schuermann, Mater. Sci. Eng. A378 (2004) 200–204.
[16] H.C. Lin, S.K. Wu, Scripta Metall. 26 (1992) 59–62.
[17] D.D. Dibitonto, P.T. Eubank, M.R. Patel, J. Appl. Phys. 66 (1989) 4095–4103.
[18] A.M. Gadalla, B. Bozkurt, J. Mater. Res. 7 (1992) 2853–2858.
[19] H.C. Lin, K.M. Lin, I.S. Cheng, J. Mater. Sci. 36 (2001) 399–404.
[20] J.C. Rebelo, A. Morao Dias, D. Kermer, J.L. Lebrun, J. Mater. Process. Technol. 84 (1998) 90–96.
[21] M.L. Jeswani, Wear 51 (1978) 227–236.